LETTER

doi:10.1038/nature12990

A single low-energy, iron-poor supernova as the source of metals in the star SMSS J031300.36−670839.3

S. C. Keller[1], M. S. Bessell[1], A. Frebel[2], A. R. Casey[1], M. Asplund[1], H. R. Jacobson[2], K. Lind[3], J. E. Norris[1], D. Yong[1], A. Heger[4], Z. Magic[1,5], G. S. Da Costa[1], B. P. Schmidt[1] & P. Tisserand[1]

The element abundance ratios of four low-mass stars with extremely low metallicities (abundances of elements heavier than helium) indicate that the gas out of which the stars formed was enriched in each case by at most a few—and potentially only one—low-energy supernova[1–4]. Such supernovae yield large quantities of light elements such as carbon but very little iron. The dominance of low-energy supernovae seems surprising, because it had been expected that the first stars were extremely massive, and that they disintegrated in pair-instability explosions that would rapidly enrich galaxies in iron[5]. What has remained unclear is the yield of iron from the first supernovae, because hitherto no star has been unambiguously interpreted as encapsulating the yield of a single supernova. Here we report the optical spectrum of SMSS J031300.36−670839.3, which shows no evidence of iron (with an upper limit of $10^{-7.1}$ times solar abundance). Based on a comparison of its abundance pattern with those of models, we conclude that the star was seeded with material from a single supernova with an original mass about 60 times that of the Sun (and that the supernova left behind a black hole). Taken together with the four previously mentioned low-metallicity stars, we conclude that low-energy supernovae were common in the early Universe, and that such supernovae yielded light-element enrichment with insignificant iron. Reduced stellar feedback both chemically and mechanically from low-energy supernovae would have enabled first-generation stars to form over an extended period. We speculate that such stars may perhaps have had an important role in the epoch of cosmic reionization and the chemical evolution of early galaxies.

Whereas the solar spectrum contains many thousands of spectral lines due to iron and other elements, the high-resolution ($R = 28{,}000$) optical spectrum of SMSS J031300.36−670839.3 (hereafter SMSS 0313−6708) is remarkable for the complete absence of detectable iron lines. Figure 1 shows a portion of the spectrum that possesses a signal-to-noise ratio (S/N) of 100 per resolution element in the vicinity of one of the strongest iron lines (Fe I at 385.9 nm wavelength). The non-detection of iron lines places an upper limit on the iron abundance of the star, [Fe/H] < -7.1, at a 3σ confidence level. (Here $[A/B] = \log_{10}(N_A/N_B)_{star} - \log_{10}(N_A/N_B)_{\odot}$, where N_A/N_B is the number ratio of atoms of elements A and B, and the subscript $\odot$ refers to the solar value.) This upper limit is 30 times lower than the iron abundance in HE 1327−2326, which has [Fe/H] = −5.6 (ref. 2), and is the most iron-deficient star previously known.

The paucity of absorption lines in the spectrum of SMSS 0313−6708 allows us to derive the abundance of only four chemical elements. The calcium abundance is determined to be [Ca/H] = −7.0. Given that existing studies have shown that [Ca/Fe] = +0.4 for the majority of extremely metal-poor stars[6], the [Ca/H] value that we determine would be consistent with an extraordinary low iron abundance limit. We suggest below, however, that the Ca abundance in SMSS 0313−6708

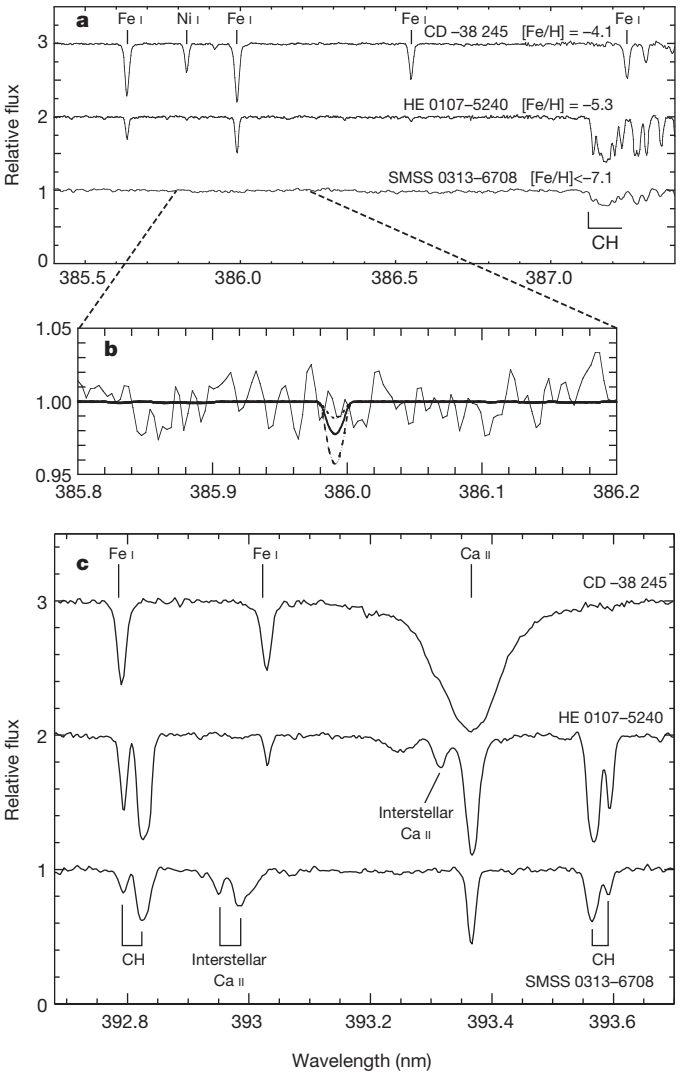

Figure 1 | A comparison of the spectrum of SMSS 0313−6708 to that of other extremely metal-poor stars. a–c, Metal-poor stars of similar temperature and surface gravity are chosen from the literature. The spectrum of SMSS 0313−6708 shows an absence of detectable Fe I lines (**a**) and is dominated by molecular features of CH (**c**). Panel **b** shows the vicinity of what should be one of the strongest iron lines in the ultraviolet/optical wavelength region. Overlaid are synthesized line profiles (1D LTE) for [Fe/H] = −7.5 (dotted line), −7.2 (solid line) and −6.9 (long dashed line).

[1]Research School of Astronomy and Astrophysics, Mount Stromlo Observatory, Cotter Road, Weston, Australian Capital Territory 2611, Australia. [2]Department of Physics, Massachusetts Institute of Technology and Kavli Institute for Astrophysics and Space Research, Cambridge, Massachusetts 02139, USA. [3]Institute of Astronomy, University of Cambridge, Madingley Road, Cambridge CB3 0HA, UK. [4]School of Mathematical Sciences, Monash University, Victoria 3800, Australia. [5]Max-Planck-Institut für Astrophysik, Karl-Schwarzschild-Strasse 1, Garching 85741, Germany.

has its origin in a specific process and no coupling to the Fe abundance is expected. Magnesium ([Mg/H] = −3.8) and carbon ([C/H] = −2.6), however, are both highly enhanced relative to iron and calcium (see Fig. 2). Table 1 presents the details of our chemical abundance analysis procedure and derived abundances and abundance limits. Figure 3 presents the abundance pattern of SMSS 0313−6708.

For the most iron-poor stars, the degree of chemical diversity increases with decreasing metallicity[6], indicative of the diversity of the few supernovae that enriched the gas before formation of these stars. Yields from supernovae with explosion energies typical of those seen in the nearby Universe are required to explain the observed abundances in stars with [Fe/H] > −3.5, except for a few elements[6]. For the most iron-poor stars, however, the supernovae required to explain the chemical abundances suggest unusual low-explosion-energy black-hole-forming events[7].

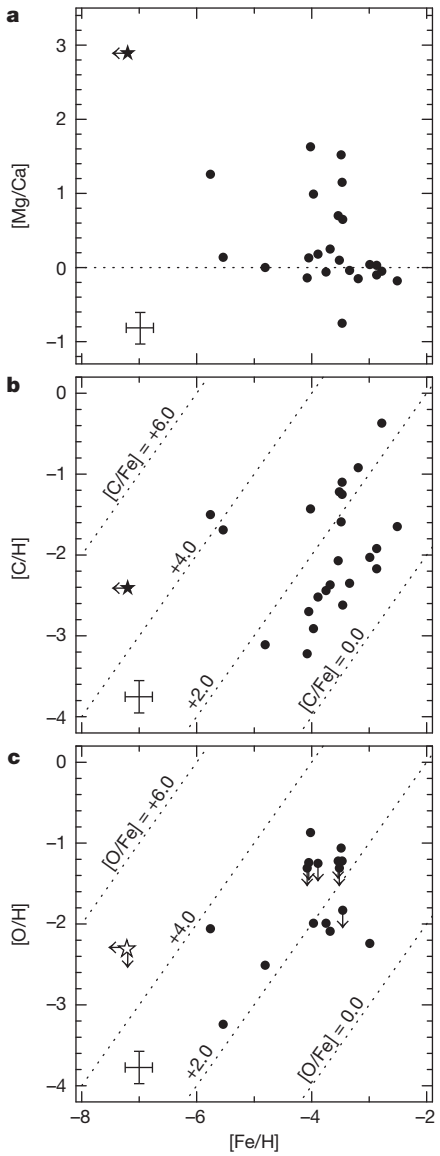

Figure 2 | A comparison of the element abundance ratios observed in SMSS 0313–6708 with those of other extremely metal-poor stars. **a**, [Mg/Ca] as a function of [Fe/H]. The dashed line is the solar abundance ratio. **b**, [C/H] as a function of [Fe/H], where dashed lines show lines of [C/Fe]. **c**, [O/H] against [Fe/H]. In each panel, our target is marked as a star symbol, and data from extremely metal-poor carbon-enhanced stars from ref. 23 are plotted as filled circles. Indicative 1 s.d. error bars are shown at bottom left in each panel. For consistency with the data from table 4 of ref. 23, the 1D LTE abundances for SMSS 0313−6708 are plotted.

Stochastic models of galactic chemical evolution that invoke low-explosion-energy supernovae[8] with a burst of formation of population III stars over the redshift range 25–17 reveal that stars such as SMSS 0313−6708 are the result of star formation in gas enriched by only one population III supernova. Whereas more iron-rich stars ([Fe/H] > −4.5) may be interpreted as composites of supernovae yields, galactic chemical evolution models show that stars with the iron abundance of SMSS 0313−6708 follow from a single supernova event.

We have compared the abundance pattern of SMSS 0313−6708 to the nucleosynthetic yields of model population III supernovae over a range of progenitor mass, explosion energy and internal mixing[9]. We find that a 1.8×10^{51} erg explosion of a $60M_{\odot}$ star of primordial initial composition with a small amount of ejecta mixing due to Rayleigh–Taylor instabilities[10] is the optimal match to the observed abundance pattern (see Fig. 3). In this model, a central black hole is formed into which the core of the massive star is subsumed. The extensive fallback of material into the black hole traps the centrally located iron and other heavy elements synthesized during the star's lifetime. Lighter elements, for example carbon and magnesium, residing at larger radii within the supernova progenitor are dispersed in the explosion.

The observed abundance pattern of SMSS 0313–6708 does not support supernova progenitors outside the mass range 10–70 $M_{\odot}$. Supernovae of mass less than $10M_{\odot}$ release large amounts of iron, and those of greater than $70M_{\odot}$ do not produce the observed carbon enhancement and lead to excessive nitrogen[9]. In particular, pair-instability supernovae are expected to yield [C/Fe] ≈ 0, rather than the [C/Fe] > 4.5 observed[10].

Our observations argue against a significantly non-axisymmetric supernova, such as one in which much of the explosion energy is channelled into a jet, because this would entrain and eject material from the core region. Any appreciable jet would lower [Mg/Fe] below that observed[11]. Furthermore, the relatively low nitrogen abundance (implied by the upper limit on that quantity), compared to carbon, suggests a slowly rotating progenitor star[12].

Interestingly, the calcium released in our model of a $60M_{\odot}$ progenitor is not synthesized in the supernova explosion itself; rather, it is produced during the stable hydrogen-burning phase. In the metal-free progenitor, thermal equilibrium is obtained only once the core of the star attains significantly higher temperature and density compared with metal-rich stars. Under such conditions, the triple-alpha process enables the synthesis of small amounts of carbon, nitrogen and oxygen

Table 1 | Chemical abundances of SMSS 0313−6708

Element X	$[X/H]_{1D,\ LTE}$	$[X/H]_{<3D>}$
Li I	0.7*	0.7*
C (CH)	−2.4	−2.6†
N (NH)	<−3.5	<−3.9†
O I	<−2.3	<−2.4†
Na I	<−5.5	<−5.5‡
Mg I	−4.3	−3.8‡
Al I	<−6.2	
Si I	<−4.3	
Ca II	−7.2	−7.0‡
Sc II	<−5.0	
Ti II	<−6.3	
V II	<−3.3	
Cr I	<−6.3	
Mn I	<−5.8	
Fe I	<−7.3	<−7.1‡
Co I	<−4.9	
Ni I	<−6.4	
Cu I	<−3.5	
Zn I	<−3.4	
Sr II	<−6.7	
Ba II	<−6.1	
Eu II	<−2.9	

Abundance ratios for SMSS 0313−6708 as derived from our Magellan/MIKE spectra. Typical (1σ) observational uncertainties in the quoted abundances are 0.1 decades in metallicity, except in the case of C and N where 0.2 is appropriate.
* Lithium abundance is expressed as $A(\mathrm{Li}) = \log_{10}(N(\mathrm{Li})/N(\mathrm{H}) + 12$.
† Abundances based on <3D>, LTE calculations.
‡ Abundances based on <3D>, NLTE calculations.

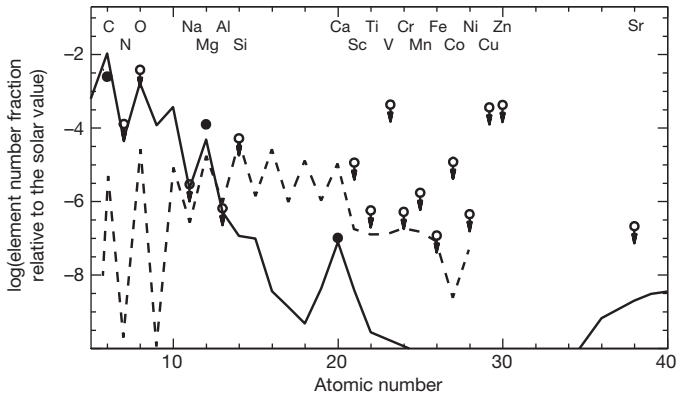

Figure 3 | The element abundance pattern for SMSS 0313−6708 compared to model values. Determined abundances are shown as filled symbols (observational uncertainties are smaller than the symbol size). Owing to the paucity of observable absorption lines, the majority of abundances are 3σ upper limits (open circles). The solid line shows the abundances predicted for a $60M_{\odot}$ population III star of relatively low explosion energy (1.8×10^{51} erg) and low levels of internal mixing (see ref. 10 for details). The dashed line shows the expected yield from a $200M_{\odot}$ supernova (with a pair-instability explosion mechanism). Such a massive progenitor leads to a [Mg/Ca] ratio that is much lower than that observed.

that subsequently catalyse the CNO energy production cycle[13]. Calcium production is the result of breakout from the CNO cycle[14]. As a consequence, we expect the calcium abundance to be decoupled from those of heavier elements in the most metal-poor stars. Such synthesis is only appreciable in initially metal-free stars where internal temperatures are sufficiently elevated.

Including SMSS 0313−6708, there are now five stars known with [Fe/H] < -4.5. The metallicity distribution function of stars reflects the integrated iron production from previous generations of supernovae. A simple model of instantaneous gas mixing[15] shows that the number of stars at a given low metallicity drops by a factor of ten for each factor of ten reduction in [Fe/H]. This simple model proves appropriate[6] for [Fe/H] $> \sim -4$. With the addition of SMSS 0313−6708, the five most iron-poor stars span a range in iron abundance of at least 2.5 decades in metallicity. The probability of such an observed metallicity density function arising from the simple model by chance is low (<1.6%; assuming they are drawn from a completeness-corrected sample normalized to the known 30 stars with $-4.0 <$ [Fe/H] < -3.5). This suggests that for [Fe/H] < -4.5 the assumption of instantaneous mixing of star-forming gas no longer holds.

The rate of mixing and enrichment from population III supernovae has an important effect on the epoch of reionization. Studies have highlighted that galaxies at $z = 6$–8 do not produce sufficient ionizing photons to lead to the reionization of the intergalactic medium[16]. With a mass function dominated by massive stars, population III stars produce about ten times the ionizing radiation over their lifetimes compared with population II stars that constitute the observable galaxies at $z = 6$–8. Prodigious radiation output by population III stars at $z \approx 20$ offers a potential resolution to the ionizing radiation shortfall.

However, simulations of the early Universe that include energetic pair-instability supernovae result in very rapid mixing of supernova ejecta, leading to the pollution of large volumes of gas with metals. This would rapidly terminate formation of population III stars, and hence population III would be extinguished before it contributed significant ionizing radiation[17]. On the other hand, supernovae with low explosion energy and low metal yield, which our observations reveal, would result in slow mixing and enrichment of the interstellar medium. This would enable the formation of population III stars over a protracted time, thus allowing the population to release substantial ionizing radiation that could potentially account for the apparent radiation shortfall, although we are unable to quantify this at present.

METHODS SUMMARY

SMSS 0313−6708 is located at right ascension 03 h 13 min 00.4 s, declination −67° 08′ 39″ (equinox 2000) and has an apparent visual magnitude $V = 14.7$. It was discovered in the continuing SkyMapper Southern Sky Survey[18]. Stellar parameters were determined from low-resolution spectrophotometry to be effective temperature $T_{\rm eff} = 5{,}125$, and surface gravity $\log g = 2.3$ (with g in cgs units; Extended Data Fig. 1). We adopt a microturbulent velocity of 2.0 km s^{-1} (the derived abundances are not sensitive to this choice). The temperature and gravity are consistent with the stellar hydrogen line profiles and the derived lithium abundance (Extended Data Fig. 2). The uncertainty in temperature is of the order of 100 K, and for surface gravity it is 0.2. Two model atmospheres are considered as the basis for abundance analysis; a Castelli–Kurucz one-dimensional hydrostatic model[19], and a spatially and temporally averaged three-dimensional hydrodynamical model from the Stagger grid[20] which we denote <3D>. Corrections for departures from local thermodynamic equilibrium (NLTE) are computed for the <3D> model following ref. 21. The abundances of Li, C and upper limits for N and O have been derived from spectrum synthesis of the lithium 670.7 nm doublet, the carbon G-band, an NH band (336.0 nm), and [O I] at 630 nm, respectively. Apart from the molecular features due to CH, only one Ca II (393 nm), one Li I (671 nm), and five Mg I (382.9, 383.2, 383.8, 517.2 and 518.4 nm) lines are detectable in our high S/N spectrum. Solar abundances for elements are from ref. 22. The upper limit to the iron abundance in the star (Fig. 1 and Extended Data Fig. 3) was determined through Markov Chain Monte Carlo analysis of addition of the strongest iron lines.

Online Content Any additional Methods, Extended Data display items and Source Data are available in the online version of the paper; references unique to these sections appear only in the online paper.

Received 9 July; accepted 5 December 2013.
Published online 9 February 2014.

1. Christlieb, N. *et al.* A stellar relic from the early Milky Way. *Nature* **419,** 904–906 (2002).
2. Frebel, A. *et al.* Nucleosynthetic signatures of the first stars. *Nature* **434,** 871–873 (2005).
3. Norris, J. E. *et al.* HE 0557–4840: ultra-metal-poor and carbon-rich. *Astrophys. J.* **670,** 774–788 (2007).
4. Caffau, E. *et al.* An extremely primitive halo star. *Nature* **477,** 67–69 (2011).
5. Hirano, S. *et al.* One hundred first stars: protostellar evolution and the final masses. *Astrophys J.* (in the press); preprint at http://arXiv.org/abs/1308.4456 (2013).
6. Yong, D. *et al.* The most metal-poor stars. II. Chemical abundances of 190 metal-poor stars including 10 new stars with [Fe/H]<-3.5. *Astrophys. J.* **762,** 27 (2013).
7. Umeda, H. & Nomoto, K. First-generation black-hole-forming supernovae and the metal abundance pattern of a very iron-poor star. *Nature* **422,** 871–873 (2003).
8. Karlsson, T., Bromm, V. & Bland-Hawthorn, J. Pregalactic metal enrichment: the chemical signatures of the first stars. *Rev. Mod. Phys.* **85,** 809–848 (2013).
9. Heger, A. & Woosley, S. E. The nucleosynthetic signature of Population III. *Astrophys. J.* **567,** 532–543 (2002).
10. Joggerst, C. C., Woosley, S. E. & Heger, A. Mixing in zero- and solar-metallicity supernovae. *Astrophys. J.* **693,** 1780–1802 (2009).
11. Tominaga, N. *et al.* The connection between gamma-ray bursts and extremely metal-poor stars: black hole-forming supernovae with relativistic jets. *Astrophys. J.* **657,** L77–L80 (2007).
12. Ekström, S., Maeder, G., Chiappini, C., Hirschi, R. & Maeder, A. Effects of rotation on the evolution of primordial stars. *Astron. Astrophys.* **489,** 685–698 (2008).
13. Ezer, D. & Cameron, A. G. W. The evolution of hydrogen-helium stars. *Astrophys. Space Sci.* **14,** 399–421 (1971).
14. Wiescher, M., Gorres, J. & Schatz, H. Break-out reactions from the CNO cycles. *J. Phys. G* **25,** 133–161 (1999).
15. Hartwick, F. D. A. The chemical evolution of the Galactic halo. *Astrophys. J.* **209,** 418–423 (1976).
16. Robertson, B. E. *et al.* New constraints on cosmic reionization from the 2012 Hubble ultra deep field campaign. *Astrophys. J.* **768,** 71 (2013).
17. Kulkarni, G., Hennawi, J. F., Rollinde, E. & Vangioni, E. Chemical constraints on the contribution of Population III stars to cosmic reionization. Preprint at http://arXiv.org/abs/1310.0684 (2013).
18. Keller, S. C. *et al.* The SkyMapper telescope and the southern sky survey. *Publ. Astron. Soc. Aust.* **24,** 1–12 (2007).
19. Castelli, F. & Kurucz, R. L. New grids of ATLAS9 model atmospheres. Preprint at http://arXiv.org/abs/astro-ph/0405087 (2004).
20. Magic, Z. *et al.* The Stagger grid: a grid of 3D stellar atmosphere models. *Astron. Astrophys.* **557,** A26 (2013).
21. Lind, K., Asplund, M. & Barklem, P. Departures from LTE for neutral Li in late-type stars. *Astron. Astrophys.* **503,** 541–544 (2009).
22. Asplund, M., Grevesse, N., Sauval, A. J. & Scott, P. The chemical composition of the Sun. *Annu. Rev. Astron. Astrophys.* **47,** 481–522 (2009).
23. Norris, J. E. *et al.* The most metal-poor stars. IV. The two populations with [Fe/H] <~-3.0. *Astrophys. J.* **762,** 28 (2013).

Acknowledgements Australian access to the Magellan Telescopes was supported through the National Collaborative Research Infrastructure Strategy of the Australian Federal Government. M.A., M.S.B., A.R.C., G.D.C., S.K., J.E.N. and D.Y. acknowledge the

support of Australian Research Council (grants DP120101237, DP0984924, DP0878137 and LF0992131). A.F. acknowledges support from NSF grant AST-1255160. A.R.C. acknowledges support from the Australian Prime Minister's Endeavour Award Research Fellowship. K.L. acknowledges support from the European Union FP7 programme through ERC grant number 320360.

Author Contributions The SkyMapper telescope was developed by B.P.S., G.S.D., M.S.B., P.T. and S.C.K. The SkyMapper data reduction procedure required to provide calibrated photometry from which the star was drawn was developed by S.C.K. M.S.B. obtained the intermediate-resolution spectrum and drew the target to the team's attention. H.R.J., A.R.C., A.F. and S.C.K. obtained the high-resolution spectrum of the target, reduced the data and performed the chemical abundance analysis using the spectral analysis package developed by A.R.C. The MCMC calculations to provide the upper limit to [Fe/H] were performed by A.R.C. K.L. performed NLTE calculations, Z.M. and M.A. constructed the <3D> atmosphere models, and A.H. the supernova models. B.P.S., A.H. and D.Y. contributed to supernova yields and MDF analysis. All authors discussed the results and commented on the manuscript.

Author Information Reprints and permissions information is available at www.nature.com/reprints. The authors declare no competing financial interests. Readers are welcome to comment on the online version of the paper. Correspondence and requests for materials should be addressed to S.C.K. (stefan.keller@anu.edu.au).

METHODS

Discovery. SMSS 0313−6708 is located at RA = 03 h 13 min 00.4 s, dec. = −67° 08′ 39″ (equinox 2000) and has an apparent visual magnitude $V = 14.7$. On the basis of photometry obtained with the SkyMapper telescope[18] on 2 October 2012, the star was predicted to be of particularly low metallicity. The SkyMapper telescope utilizes a novel filter set that places tight constraints on the fundamental properties of the stars surveyed, namely effective temperature, surface gravity and stellar metallicity.

Abundance analysis. Two model atmospheres are considered as the basis for abundance analysis; a Castelli–Kurucz 1D hydrostatic model[19], and a spatially and temporally averaged 3D hydrodynamical model from the Stagger grid[20] which we denote <3D>. Corrections for departures from local thermodynamic equilibrium (NLTE) are computed for the <3D> model following ref. 21. The abundances of Li and C and upper limits for N and O have been derived from spectrum synthesis of the lithium 670.7 nm doublet, carbon G-band, NH band (336.0 nm), and [O I] at 630 nm, respectively. Apart from the molecular features due to CH, only one Ca II (393 nm), one Li I (671 nm) and 5 Mg I (382.9, 383.2, 383.8, 517.2 and 518.4 nm) lines are detectable in our high S/N spectrum. Solar abundances for elements are from ref. 22. Observational uncertainties in the derived abundances (Table 1) are 0.1 decades in metallicity. The local S/N ratio in the observed spectrum governs the uncertainty. In the case of upper limits to abundance, these were determined by matching synthesized spectra to the local average minima in the vicinity of the line in question. Observational uncertainties are larger in the case of C and N ($\sigma = 0.2$ decades in metallicity) where synthetic spectra are compared to the multiple features of molecular bands.

Medium-resolution spectroscopy. The star's extremely metal-poor status was confirmed through medium-resolution spectroscopy with the WiFeS spectrograph[24] on the ANU 2.3 m telescope on 2 January 2013.

High-resolution spectroscopy. We observed SMSS 0313−6708 on five different nights (namely 23–25 January and 6–7 February 2013) with the Magellan Inamori Kyocera Echelle (MIKE) spectrograph[25] at the 6.5 m Magellan Clay telescope, Chile. All observations were taken using a 1.0" slit, providing a spectral resolution of $R = 28{,}000$ in the blue arm and $R = 22{,}000$ in the red arm. Calibration frames were taken at the start of each night, including 20 flat-field frames and 10 Th-Ar arc lamp exposures for wavelength calibration. Data reduction used the Carpy data reduction pipeline[26]. Each reduced echelle order was carefully normalized using a third order spline with defined knot spacing. Normalized orders were stitched together to provide a single one-dimensional spectrum from 336 to 940 nm.

Adopted stellar parameters. The WiFeS/ANU 2.3 m spectrum was flux calibrated by comparison with spectrophotometric standard stars as described in ref. 27. Model atmosphere fluxes in ref. 28 were then compared to those observed from SMSS 0313−6708 as described in ref. 29 to determine the best match to the spectrum. Extended Data Fig. 1 shows the result of the fit to SMSS 0313−6708. We have adopted the $T_{\rm eff}$ and $\log g$ resulting from this analysis in the subsequent abundance analysis: $T_{\rm eff} = 5{,}125$ K, and surface gravity $\log g = 2.3$ [cgs]. We adopt a microturbulent velocity of 2.0 km s^{-1} (the derived abundances are not sensitive to this choice). To confirm that the values used are appropriate, we have made a comparison between the Balmer line profiles observed and those of stars with bracketing $T_{\rm eff}$ and $\log g$ observed with the same instrument and settings (seen in Extended Data Fig. 2 a, b). The uncertainty in temperature is of the order of 100 K, and for surface gravity it is 0.2.

Lines of interstellar absorption of Ca-K and Na-D are apparent in the spectrum. We determine the equivalent width of the Na-D1 line to be 10.9 pm. The relation between equivalent width and interstellar reddening from ref. 30 provides $E(B-V) = 0.04 \pm 0.01$ which we adopt. Using the infrared flux method for the $BVJHK$ system[31] (BV photometry from APASS[32]; JHK from 2MASS[33]) we derive a photometric temperature of $T_{\rm eff} = 5{,}210 \pm 64$ K. From utilization of $griJHK$[31] (gri from APASS) we determine $T_{\rm eff} = 5{,}265 \pm 76$ K. These values and those determined through spectrophotometric analysis are in concordance.

Lithium. Lithium is detected in the star at a level $A(\mathrm{Li}) = \log_{10}(N(\mathrm{Li})/N(\mathrm{H}) + 12 = 0.7$ that displays significant depletion from the primordial Big Bang level ($A(\mathrm{Li}) = 2.72$)[34]. Such lithium depletion is expected within a metal-poor first ascent red giant branch star[21] due to cycling of material in regions of high temperature where lithium is destroyed and subsequent dilution in an extensive convective envelope. This evolutionary status is in line with the adopted $\log g$ for SMSS 0313−6708.

Derivation of upper limit on iron abundance. An upper limit to the iron content has been calculated from a Markov Chain Monte Carlo analysis. The emcee package[35] was used, which is a Python (http://www.python.org) implementation of an affine-invariant ensemble sampler[36]. Walkers (200) were used to explore the parameter space and maximize the log-likelihood. The likelihood function computes synthetic spectra using the MOOG code[37] and a 1D model atmosphere[19] for SMSS 0313−6708 ($T_{\rm eff} = 5{,}125$ K, $\log g = 2.3$, [Fe/H] = −5, microturbulent velocity $v_{\rm t} = 2$ km s^{-1}) and compares it to portions of the normalized observed spectrum. The spectral regions surrounding the Fe lines at 385.9 nm and 371.9 nm were synthesized for different Fe abundances, smoothed with a Gaussian kernel (FWHM = 9.6 km s^{-1}) to match the observations, and shifted to zero wavelength before being stacked. With logarithmic oscillator strengths of −0.431 and −0.710 respectively, these excitation potential $\chi_{\rm exc} = 0.0$ eV transitions are the strongest Fe absorption lines available from our near-ultraviolet to infrared spectrum. The observed spectrum surrounding these Fe lines is similarly stacked with uncertainties added in quadrature based on the S/N of individual spectra, allowing for the χ^2 difference between the model and observed spectra to be calculated. This model includes five free parameters: noise jitter, a constant scaling value for the stacked normalized spectrum, a residual velocity offset for each absorption line, and Fe/H. Using linear metallicity as a parameter (instead of logarithmic metallicity [Fe/H]) allows for both positive and approximate negative (that is, emission spectra) column depths.

A uniform prior between [0, 1] was used for the noise jitter, and a uniformly distributed linear prior between [Fe/H] = −5.5 to −4.5 was adopted for metallicity. As the observed spectra is already at rest-frame and the laboratory wavelengths of these transitions are very well known, the velocity offset for each transition was treated as a Gaussian prior with mean = 0 and s.d. = 0.5 km s^{-1}. The continuum scaling factor prior was also treated as a Gaussian distribution, with mean = 1, s.d. = 0.02. After 600 walker steps, an asymptotically-approaching mean acceptance fraction of 0.369 and a minimum reduced χ^2 of 1.49 was observed. The resultant 67.8%, 95% and 99.7% upper limits for $[\mathrm{Fe/H}]_{\rm 1D,LTE}$ are <−7.7, <−7.5 and <−7.3. This is demonstrated in Extended Data Fig. 3, where stacked synthetic spectra for each metallicity is overlaid upon the stacked observed spectrum for the Fe lines used. After corrections for 3D and non-LTE effects, the 99.7% upper limit becomes $[\mathrm{Fe/H}]_{\rm 3D,NLTE} = <-7.1$.

24. Dopita, M. A. *et al.* The wide field spectrograph (WiFeS): performance and data reduction. *Astrophys. Space Sci.* **327,** 245–257 (2010).
25. Bernstein, R., Shectman, S. A., Gunnels, S. M., Mochnacki, S. & Athey, A. E. MIKE: A Double Echelle Spectrograph for the Magellan Telescopes at Las Campanas Observatory. *SPIE Conf. Ser.* **4841,** 1694–1704 (2003).
26. Carnegie. Observatories Software Repository. MIKE pipeline http://code.obs.carnegiescience.edu/mike (2012).
27. Bessell, M. S. Measuring the Balmer Jump and the effective gravity in FGK stars. *Publ. Astron. Soc. Pacif.* **119,** 605–615 (2007).
28. Gustafsson, B. *et al.* A grid of MARCS model atmospheres for late-type stars. I. methods and general properties. *Astron. Astrophys.* **486,** 951–970 (2008).
29. Norris, J. E. *et al.* The most metal-poor stars. IV. The two populations with [Fe/H] <∼-3.0. *Astrophys. J.* **762,** 28 (2013).
30. Munari, U. & Zwitter, T. Equivalent width of Na I and K I lines and reddening. *Astron. Astrophys.* **318,** 269–274 (1997).
31. Casagrande, L., Ramirez, I., Melendez, J., Bessell, M. & Asplund, M. An absolutely calibrated $T_{\rm eff}$ scale from the infrared flux method. Dwarfs and subgiants. *Astron. Astrophys.* **512,** A54–A64 (2010).
32. Henden, A. A. *et al.* The AAVSO Photometric All-Sky Survey DR7 http://www.aavso.org/apass (2013).
33. Skrutskie, M. F. *et al.* The Two Micron All Sky Survey (2MASS). *Astron. J.* **131,** 1163–1183 (2006).
34. Coc, A., Goriely, S., Xu, Y., Saimpert, M. & Vangioni, E. Standard Big Bang nucleosynthesis up to CNO with an improved extended nuclear network. *Astrophys. J.* **744,** 158 (2012).
35. Foreman-Mackey, D., Hogg, D. W., Lang, D. & Goodman, J. emcee: The MCMC hammer. *Publ. Astron. Soc. Pacif.* **125,** 306–312 (2013).
36. Goodman, J. & Weare, J. Ensemble samplers with affine invariance. *Commun. Appl. Math. Comput. Sci.* **5,** 65–80 (2010).
37. Sneden, C. http://www.as.utexas.edu/~chris/moog.html (2013).

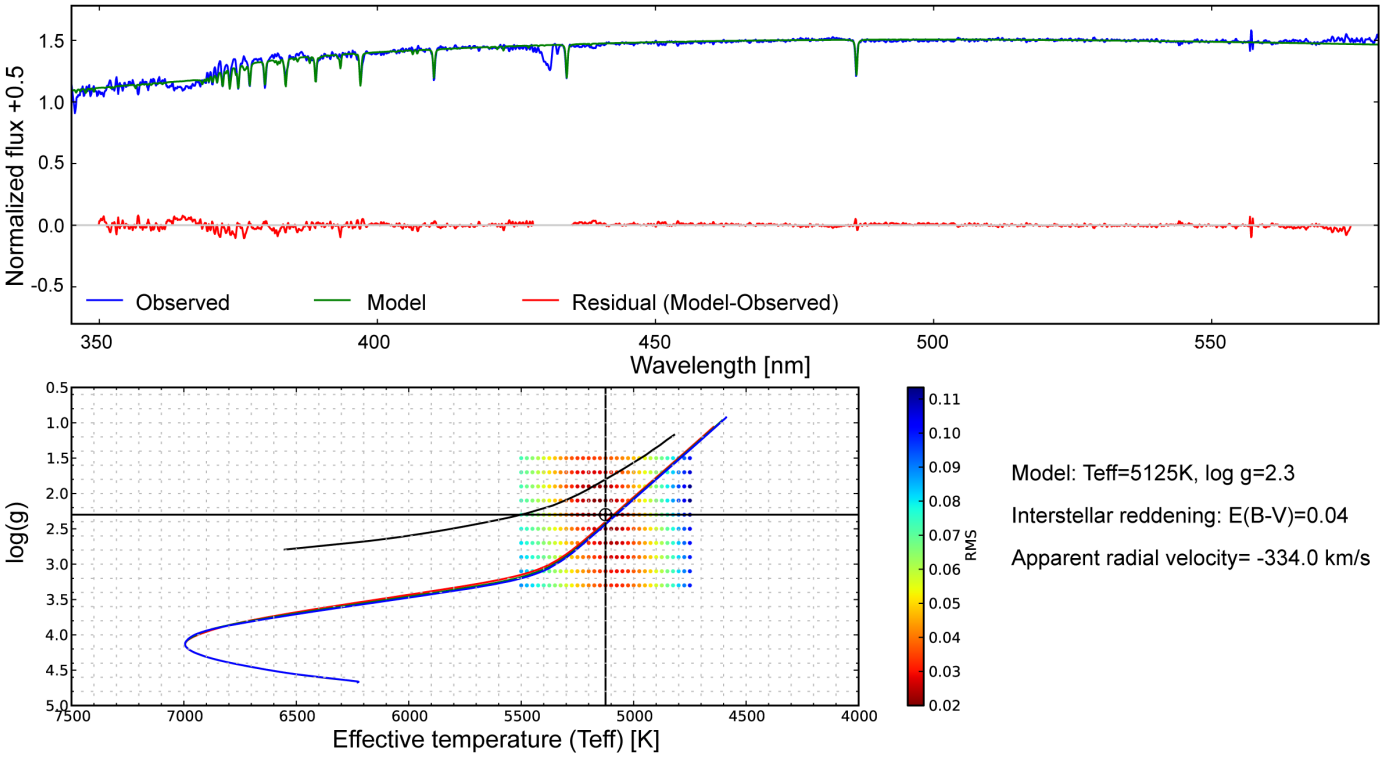

Extended Data Figure 1 | The summary of spectrophotometric analysis of SMSS 0313−6708. In the top frame, the blue line shows the observed spectrum and the green line is the best-fitting model spectrum. The red line beneath shows the residual spectrum. In the lower frame, the cross-hair marks the location of the best-fitting $T_{\rm eff}$ and log g and the r.m.s. values of the fit are represented in colour for a subgrid. Halo isochrones are shown to assist in the selection of the most likely parameters. The interstellar reddening is found to be $E(B-V) = 0.04$.

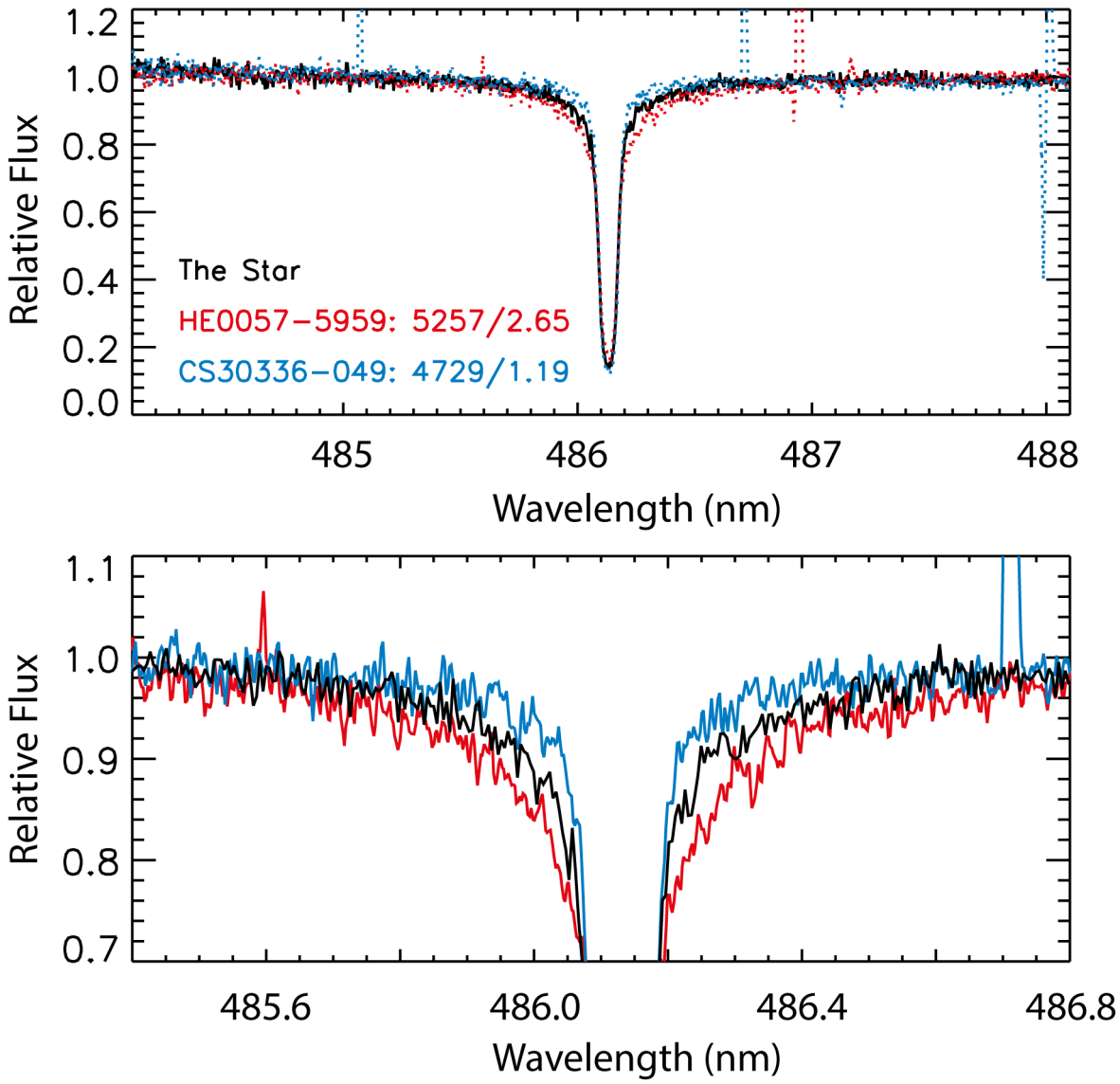

Extended Data Figure 2 | The comparison of the Hβ Balmer line profile of SMSS 0313−6708 to stars of bracketing stellar parameters reported in the literature. We use this comparison as a qualitative verification of the stellar parameters for SMSS 0313−6708 determined from spectrophotometric analysis. Literature values for $T_{\rm eff}$ and log g respectively are stated in the top panel adjacent to the star identifier. The top panel shows a comparison of the intensity in the vicinity of the Hβ Balmer line for SMSS 0313−6708 (black line), HE 0057−5959 (red line) and CS 30336−049 (blue line). The bottom panel is an enhanced zoom to show the line profile wings.

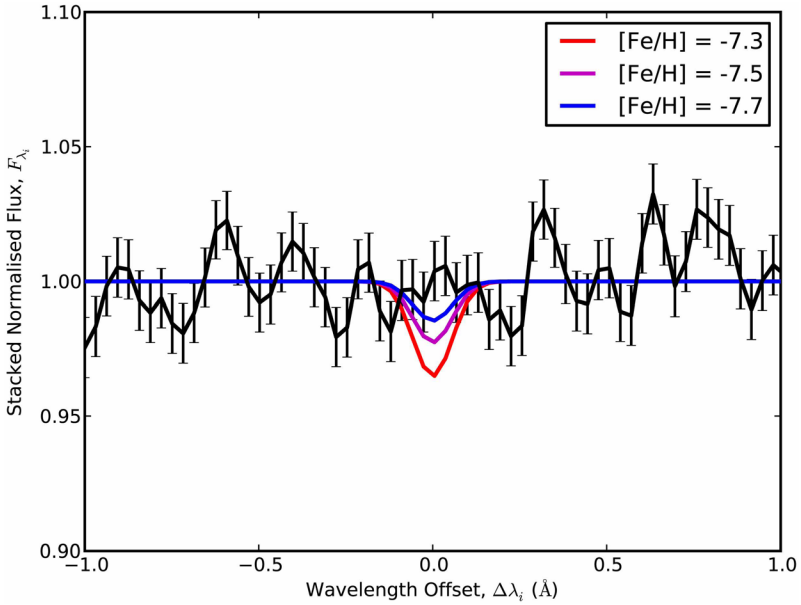

Extended Data Figure 3 | Determination of upper limits to the iron abundance. The black line with associated uncertainties (error bars, s.d.) is the observed spectrum stacked in the vicinity of the strongest iron lines. The coloured lines show 67.8% (blue), 95% (magenta) and 99.7% (red) confidence upper limits for $[Fe/H]_{1D,NLTE}$. The vertical axis is the normalized spectral intensity formed from the addition of regions of spectrum centred on strong iron lines (2 Å wide). The horizontal axis is the wavelength shifted such that each iron line lies at the origin.